Optical and Photoelectrical Properties of $(CdTe)_{100-x}(SbS)_x$ thin films

K. A. ALY[a,b*], A. DAHSHAN[c,d]
[a]*Physics Department, Faculty of Science and Arts, Jeddah University,Jeddah, SA.*
[b]*Physics Department, Faculty of Science, Al–Azhar, University, Assiut Branch, Assiut, Egypt.*
[c]*Department of Physics, Faculty of Science, Port Said, University, Port Said, Egypt.*
[d]*Department of Physics - Faculty of Girls - King Khalid University Abha, Saudi Arabia.*

The present work deals with the effect of the addition of SbS at the expense of CdTe content on the optical, electrical and photo electrical properties of polycrystalline $(CdTe)_{100-x}(SbS)_x$ ($0 \le x \le 28$ at.%) thin films. Increasing the SbS content is found to affect the dispersion parameters and energy gap of the films. The transmission spectra, $T(\lambda)$, of the films at normal incidence were obtained in the spectral region (400-2500 nm). A straightforward analysis proposed by Swanepoel has been applied to derive the complex index of refraction (real and imaginary parts) and the film thickness with high accuracy. The optical absorption mechanism in the films under study obeys the allowed direct transitions. The optical band gap of $(CdTe)_{100-x}(SbS)_x$ films are decreased from 1.58 to 1.33 eV with increasing SbS content from 0 to 28 at.%. Both of Wemple–DiDomenico and Solomon dispersion relationships were used to obtain the dispersion parameters of the films. The composition dependence of steady state dark and photo conductivities at room temperature shows that the dark and the photo conductivities increase while the activation energies for dark and photoconduction decrease with increasing the SbS content.

(Received March 16, 2015; accepted September 9, 2015)

Keywords: Thin films, Polycrystalline, Optics, Photoconductivity

1. Introduction

Chalcogenides are of great interest to researchers because of their flexible structure, wide range of properties, capacity for doping, and especially their ability to transmit light in the mid- to far-infrared region of the spectrum [1]. They generally show a wide variation in the refraction index depending on their chemical composition [2], as well as a capacity to tune many important physical and optical properties.

The study of the photoconductivity (PC) provides an understanding of the photo generations and the transport of the free carriers. The PC represents a valuable tool in understanding the recombination kinetics which, in turn, provides information about the localized states in the chalcogenide materials [3, 4]. The PC properties of several chalcogenides have been investigated by many workers [5-9].

Optical properties of chalcogenide thin films have been the subject of intense studies during the last decades specially the determination of the optical constants which frequently based on the optical transmission spectra at normal incidence [10-13]. Simple methods, which do not require any previous knowledge of the thickness of the films, are fairly accurate, with the thickness and refractive index being determinable to within about 1% [11]. They do, however, assume that the film has a uniform thickness which, when not the case, leads to less accurate results and even serious errors.

The present work is concerned with the analysis of the optical properties of the as-deposited polycrystalline $(CdTe)_{100-x}(SbS)_x$ (where x = 0, 8, 16, 20 and 28 at. %) thin films. The method proposed by Swanepoel [11], which is based on the use of maxima and minima of the interference fringes in the transmission spectrum, has been used to obtain the refractive index and the film thickness in the weakly absorbing and transparent regions of the spectrum. The absorption coefficient and the extinction coefficient have been determined from transmission spectra in the strong absorption region. In addition, the dc dark and photo conductivities of the films are considered.

To the best of our knowledge, there has been no thorough study of optical and photoelectrical properties of the $(CdTe)_{100-x}(SbS)_x$ thin films. The lack of data in the literature concerning the optical and photoelectrical characterization of films of these particular materials, along with their attractive potential technological applications, highlights the significance of the present investigation.

2. Experimental details

Different compositions of bulk $(CdTe)_{100-x}(SbS)_x$ (where $0.0 \le x \le 28$ at. %) materials were prepared starting with their components of high purity (99.999 %) by the melt-quenching technique [13-16]. Thin films were prepared by thermal evaporation of small ingot pieces onto chemically cleaned glass substrates (microscope slides).

The thermal evaporation process was performed inside a coating (Edward 306E) system at a pressure of approximately 10^{-3} Pa. During the deposition process (at normal incidence), the substrates were suitably rotated in order to obtain films of uniform thickness. The evaporation rate and the film thickness were controlled using a quartz crystal monitor (DTM 100). The thicknesses of the films under study were found to be in the range 750-805 nm and the evaporation rate was 10 nm/s. The chemical compositions of the investigated specimens were checked using energy-dispersive X-ray spectroscopy (Link Analytical EDS). The films were checked using an X-ray diffractometer (Philips type 1710 with Cu as a target and Ni as a filter, $\lambda = 1.5418$ Å).

A double-beam (Jasco V-630) spectrophotometer was used to measure the transmittance for the prepared films in the wavelength range from 400 to 2500 nm. Without a glass substrate in the reference beam, the measured transmittance spectra were used to calculate the optical constants of the films. In the present work, the envelope method suggested by Swanepoel has been applied [11].

For electrical and photoelectrical measurements, two gold electrodes with a spacing of 0.001 m and length 0.014 m were deposited. Silver paste is used for making the contacts; the electrode contacts had an ohmic character as determined by current-voltage characteristics. The dark and photo conductivity measurements were carried out in the temperature range 300–400 K under vacuum of about 1.33×10^{-3} Pa. The measuring system consists of a regulated dc power Supply (Pasco, model 1030A) in series with the sample and Keithley electrometer (model 6517A). A tungsten lamp of 200 W was used for illumination. Small fluctuations in the measured photocurrent (~0.2%) were observed for the studied films. The photocurrent (I_{ph}) was determined as the difference between the currents measured with and without illumination. The intensity of the light source was measured with the help of a photocell. The current of the photocell was directly proportional to the intensity of the light.

3. Results and discussion

Figs. 1-a and 1-b show the EDX spectra for CdTe and $(CdTe)_{72}(SbS)_{18}$ films respectively as an example. The elemental compositions for $(CdTe)_{100-x}(SbS)_x$ (where x = 0, 8, 16, 20 and 28 at. %) thin films were obtained and listed in Table 1. From this table, the compositions so obtained agreed with those of the starting materials to within ± 0.55 at %.

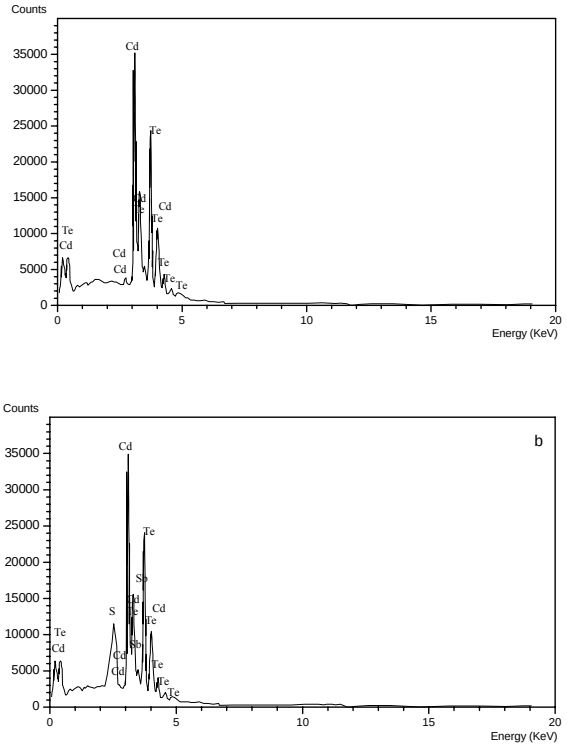

Fig. 1. a) EDX spectrum of the as prepared CdTe films b) EDX spectrum of the as prepared $(CdTe)_{72}(SbS)_{28}$ films

Table 1: Thickness and EDX Results at %. for $(CdTe)_{100-x}(SbS)_x$ ($0 \le x \le 28$ at. %) thin films.

Composition	Film thickness (nm)	EDX Results at%.			
		Cd	Te	Sb	S
CdTe	750	49.55	50.45	0.0	0.0
$(CdTe)_{92}(SbS)_8$	780	44.65	44.77	4.82	5.76
$(CdTe)_{84}(SbS)_{16}$	775	41.95	42.88	7.32	7.85
$(CdTe)_{80}(SbS)_{20}$	792	39.15	41.05	9.72	10.08
$(CdTe)_{72}(SbS)_{28}$	805	36.38	35.7	13.88	14.04

The as prepared $(CdTe)_{100-x}(SbS)_x$ films onto glass substrates were polycrystalline in nature and had a cubic type structure. The X-ray diffraction patterns of the as-deposited CdTe films displayed a strong peak associated with corresponding planes of cubic CdTe (Volume of cell: 273.36) as detected by ICDD (00-010-0207).

However, some other peaks as CdS (Volume of cell: 224.42) and $Cd_{0.3}Sb_{1.4}Te_{2.4}$ (Volume of cell: 472.43), as detected by ICDD (00-047-1179, 00-019-0191 and 00-047-1278), have been observed due to the addition of SbS as shown in Fig. 2.

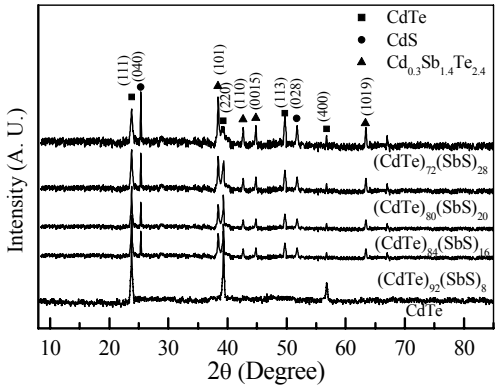

Fig.2. XRD of the as prepared (CdTe)100-x(SbS)x (0 ≤x ≤ 28 at. %) thin films

3.1 Calculation of the dispersion parameters

With the addition of SbS at the expense of CdTe in polycrystalline $(CdTe)_{100-x}(SbS)_x$ thin films a clear red shift of the optical edge of the transmittance spectra, T(λ), was observed (see Fig.3). As an example, Fig.4 represents the measured transmittance, *T*, spectra, the created envelopes T_M and T_m and the geometric mean, $T_\alpha = \sqrt{T_M T_m}$, in the spectral region with interference fringes for the CdTe thin film.

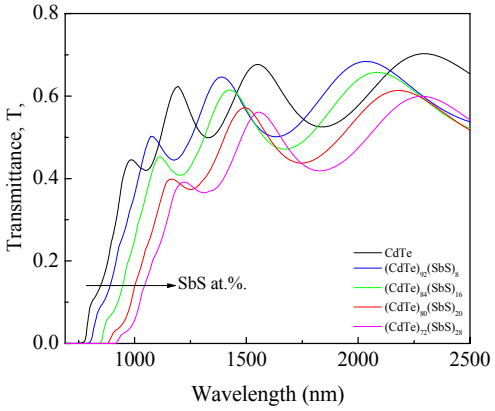

Fig.3. Transmission spectra of the polycrystalline $(CdTe)_{100-x}(SbS)_x$ (0 ≤x ≤ 28 at. %) thin films

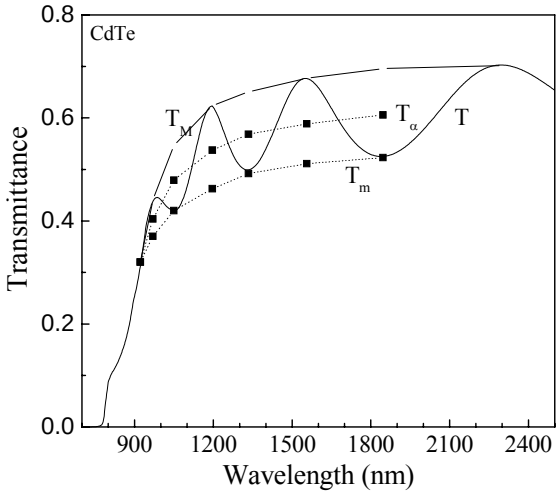

Fig.4. Transmission spectra of the as prepared CdTe thin film. The curves T_M, T_m and T_α were plotted according to the text

Based on the idea of Manifacier et al. [17] Swanepoel's method, has been applied to obtain the the film thickness and complex index of refraction for $(CdTe)_{100-x}(SbS)_x$ (where 0.0 ≤ x ≤ 28 at. %) films. The calculation details are presented in our previous papers [13, 18-21]. The calculated values of the refractive index for $(CdTe)_{100-x}(SbS)_x$ films can be fitted to a function such as the two-term Cauchy dispersion relationship [21] $n(\lambda) = a + (b/\lambda^2)$ which can be used to extrapolate the wavelength dependence beyond the range of measurement as shown in Fig. 5. As shown in this figure, the refractive index increases with increasing SbS content over the entire spectral range studied. Accrding to Fajans's rules [22] the polarizing power of the cation increases with decreasing its size and number of filled orbitals and with increasing it is positive charge, the polarizability of the anion increases with increasing its size and with increasing its negative charge. In the present study, we replace the Te and Cd atoms (the largest atomic radii (1.43 and 1.12 A^o respectively)) with the largest atomic radii Sb (1.45 A^o) atoms that, leads to increasing the electronic polarizability and consequently the refractive index of the as prepared $(CdTe)_{100-x}(SbS)_x$ (0.0 ≤ x ≤ 28 at. %) thin films.

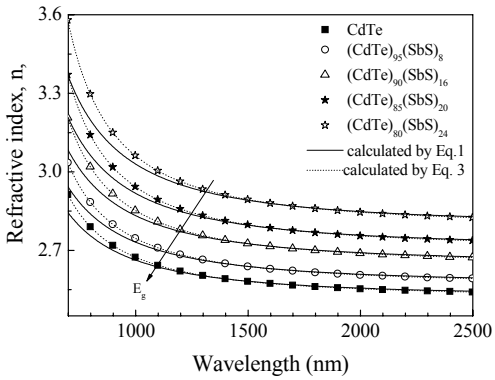

Fig.5. Refractive index dispersion spectra for $(CdTe)_{100-x}(SbS)_x$ ($0 \le x \le 28$ at. %) thin films. Dotted curves are determined according to Cauchy dispersion relationship [18]

In the range of transparency, the values of the refractive index can be fitted according to Wemple-DiDomenico (WDD) dispersion relationship [23, 24], i.e., to the single-oscillator model:

$$n^2(h\nu) = 1 + \frac{E_o E_d}{E_o^2 - (h\nu)^2} \qquad (1)$$

where, E_o is the single-oscillator energy and E_d is the dispersion energy or single-oscillator strength. By plotting $(n^2-1)^{-1}$ against $(h\nu)^2$ and fitting straight lines as shown in Fig. 6, E_o and E_d can be deduced using the intercept E_o/E_d and the slope $(E_oE_d)^{-1}$ respectively. The oscillator energy E_o is an average energy gap and, to a good approximation, scales with the optical band gap, $E_o \approx 2E_g$, as was found by Tanaka [25].

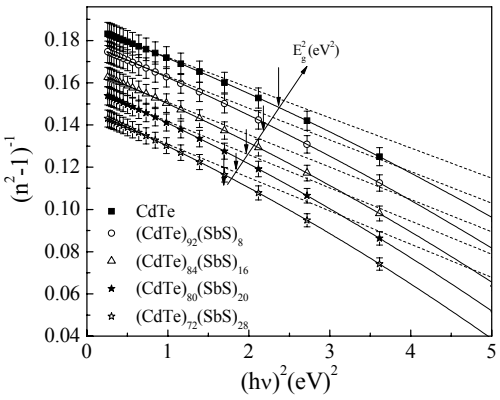

Fig.6. Plots of refractive index factor $(n^2 - 1)^{-1}$ versus $(h\nu)^2$ for $(CdTe)_{100-x}(SbS)_x$ ($0 \le x \le 28$ at. %) thin films. Dotted curves are determined according to the Wemple-DiDomenico (WDD) dispersion relationship [19] and solid curves are determined according to Solomon model [22]

Wemple–DiDomenico model describes the dielectric response for transitions below the optical gap E_g^{opt}, reducing the complex valence- and conduction-band system to a two-level system, with the simple one-oscillator formula:

$$n^2(h\nu) - 1 = (n_0^2 - 1)\frac{E_M^2}{E_M^2 - (h\nu)^2} \qquad (2)$$

where n_0 is the static refractive index (i.e. extrapolated to photon energy zero). The quantity E_M is the average energy gap parameter, that is likened in this particular model to the energy difference between the two levels of a one-oscillator system. Plotting $(n^2-1)^{-1}$ against $(h\nu)^2$ (Fig. 6) and fitting a straight line enables the determination of n_0 and E_M, directly from the slope and the intercept on the Y-axis. The deduced values of E_o, E_d, and n_0 are listed in Table 2. In this table it was noted that, E_o decreases while n_0 and E_d increase with increasing of the SbS content.

Moreover, in Fig. 6 it can be seen that, the experimental variation in the refractive index clearly departs from that given by Eq. (2), when the photon energy approaches the optical- gap value. In this case, the one-oscillator approximation fails (dotted lines), and the width of the bands induces some divergence, due to the denominator term in Eq. (2); one would expect a variation in n faster than that given by the one-oscillator formula. Nevertheless, for photon energy well below the optical gap the Wemple–DiDomenico optical dispersion relationship provides an excellent experimental fit to the measured refractive index.

An optical dispersion model has been proposed by Solomon [26], which, very importantly, takes into account the effect of the width of the bands, when the photon energy is not infinitely small compared with the optical gap, by the following relationship:

$$n^2(h\nu) - 1 = (n_0^2 - 1)\frac{1}{1 - (h\nu)^2/E_c^2 - \beta((h\nu)^4/E_c^4)} \qquad (3)$$

With $E_c^2 = E_m^2 - \Delta^2$ and $\beta = 4\Delta^2/3E_c^2$.

Considering a constant density of states from the bottom to the top of each energy band, the value of the width of the bands, Δ, will then be a quantity measuring the 'effective width' of the bands. It is important to note that this model assumes that the widths of the valence and conduction bands are equal.

A better agreement between the experimental values and this dispersion relationship is found, particularly when the photon energy approaches the value of the optical gap. The obtained values of Δ and E_M (as $E_{M(sol)}$) are listed in Table 2. The three parameters $E_g^{opt}{}_{(Sol)}$, E_M and Δ are not independent: $E_g^{opt}{}_{(Sol)} = E_M - \Delta$. Therefore, from the mentioned values of E_M and Δ, the values of the optical gap, $E_g^{opt}{}_{(Sol)}$, were estimated and listed in Table 2. The

estimated optical gap decreases with increase of the SbS content.

3.2 Determination of the extinction coefficient and optical band gap

Continuing with the description of the data processing method, when there is no substrate in the reference beam and the values of the thickness *d*, the refractive index of the film *n* and the refractive index of substrate are already known, the absorption coefficient α is derived using the well-known equation suggested by Connell and Lewis [27]. To complete the calculations of the optical constants, the extinction coefficient, *k*, is calculated using the values of α and λ by the well-known relation $k = \alpha\lambda/4\pi$. The spectral dependence of the extinction coefficient for the $(CdTe)_{100-x}(SbS)_x$ (where x = 0, 8, 16, 20 and 28 at. %) thin films is found to shift to the long wave side with the addition of SbS as shown in Fig. 7.

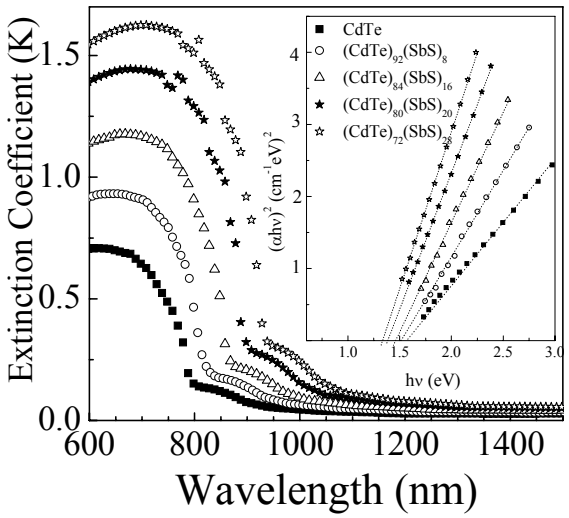

Fig.7. The extinction coefficient k vs. λ and (b) $(\alpha h\nu)^2$ vs. (hν) for $(CdTe)_{100-x}(SbS)_x$ (0 ≤x ≤ 28 at. %) thin films. Inset shows the dependence of $(\alpha h\nu)^2$ on photon energy (hν) for $(CdTe)_{100-x}(SbS)_x$ thin films

In the region of strong absorption ($\alpha \leq 10^5$ cm^{-1}) the imaginary part of the complex index of refraction is much less than *n* and the photon energy dependence of the absorption coefficient can be described by Tauc's relation [28] for allowed direct transitions, $(\alpha h\nu)^2 = B\,(h\nu - E_g)$ where *B* is a parameter that depends on the transition probability and E_g is the optical energy gap. The inset of Fig. 7 shows the absorption coefficient in the form of $(\alpha h\nu)^2$ versus $h\nu$ for $(CdTe)_{100-x}(SbS)_x$ films. The intercepts of the straight lines with the photon energy axis yield the values of the optical band gap. The obtained values of E_g^{opt} decrease with increasing SeSb content as shown in Table2.

The observed decrease in E_g^{opt} can be ascribed to the formation of $Cd_{0.3}Sb_{1.4}Te_{2.4}$ crystallites (see Fig.2). In accordance to the chemical bond approach [4, 20] the strongest Cd-Se bonds (58.78 kal.mol^{-1}) are expected to occur then Cd-Te bonds (36.72 kal.mol^{-1}) followed by Cd-Sb bonds (34.2 kal.mol^{-1}). After these bonds are formed there are excess of Sb valences that leading to the formation of defect homopolar Sb-Sb bonds (30.22 kal.mol^{-1}). The excess of homopolar Sb-Sb bonds are found to increases with increase of the SbS content (Table 2). This may be leads to an increase of the width of localized states in the band tails and therefore the optical band gap decreases [20]. The hetero-nuclear bonds like Cd-Se, Cd-Te and Cd-Sb are calculated based on the homo-nuclear bonds and the electronegativities of the constituent atoms as detailed in references 4 and 20. On the other hand when ($\alpha \leq 10^4$ cm^{-1}), the absorption coefficient α shows an exponential dependence on photon energy, *h*ν, and obeys the Urbach relation [28]

$$\ln(\alpha) = \ln(\alpha_0) + (h\nu / E_e) \qquad (4)$$

where α_o is a constant and E_e is the Urbach energy (related to the width of the band tail of the localized states at the conduction or valence band edge). Fig.8 demonstrates that the exponential behaviour of the absorption edge as determined by Eq. (4) is satisfied for our films. The obtained values of E_e are listed in Table 2. It was found that the values of E_e increases with the increase on SbS content therefore, the decrease in E_g of amorphous films can be explained by an increased tailing of the band into the gap [29]. From Table 2 it is evident that the Tauc model [28] based on the electronic transitions between the localized states in the band edge tails may well be valid for such systems

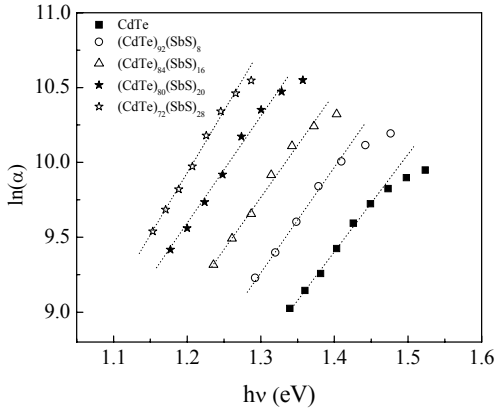

Fig .8. The absorption coefficient in the from of ln(α) vs. (hν) for $(CdTe)_{100-x}(SbS)_x$ (0 ≤x ≤ 28 at. %) thin films

Table 2: Dispersion parameters for $(CdTe)_{100-x}(SbS)_x$ ($0 \le x \le 28$ at. %) thin films.

SeSb at. %	E_o	E_d	n_o	Δ	$E_{M(Sol)}$	E_g^{opt}(Sol)	E_g^{opt}	E_g^{photo}	E_e	Exces of Sb-Sb bonds
	eV					eV			meV	
0	3.61	19.37	2.52	3.32	4.88	1.56	1.58	1.574	123	---
8	3.35	20.02	2.56	3.08	4.60	1.53	1.55	1.535	142	2
16	3.25	20.88	2.67	2.91	4.37	1.48	1.49	1.485	154	4
20	3.11	21.34	2.73	2.82	4.21	1.39	1.39	1.403	161	5
28	2.98	22.21	2.82	2.70	4.01	1.36	1.36	1.367	179	7

3.3 Steady State Photoconductivity

Fig. 9 represents the spectral distribution of dc-photoconductivity of the $(CdTe)_{100-x}(SbS)_x$ ($0 \le x \le 28$ at. %) thin films measured at room temperature, G = 1.0 and applied electric field 4 x 10^5 Vm^{-1}. From this figure, it is clear that the addition of SbS shifts the photocurrent peak into the low-energy side of the spectrum that leads to a decrease in the energy gap which, is found in good agreement with the results obtained by the optical measurements. Furthermore, the energy gap (E_g^{photo}) of the films under study can be easily determined by using the relation [4]:

$$E_g^{photo}(eV) = hc / \lambda_{1/2} \qquad (5)$$

where *h* is the Plank's constant, c is the velocity of light and $\lambda_{1/2}$ is the wavelength (nm) at which the photocurrent falls to half its maximum value. The obtained values of E_g^{photo} are listed in Table 2. The obtained values of E_g^{photo} are found to in good agreement with those obtained by optical measurements.

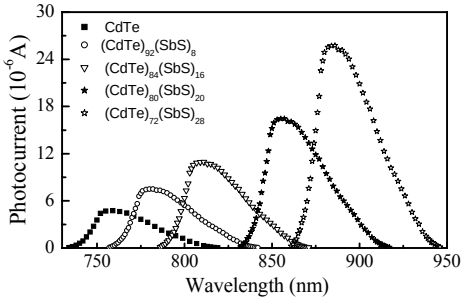

Fig.9. The spectral distribution of dc-photoconductivity of the $(CdTe)_{100-x}(SbS)_x$ ($0 \le x \le 28$ at. %) thin films measured at room temperature, G = 1.0 and applied electric field 4 x 10^5 Vm^{-1}

The dc-dark conductivity (σ_{dc}) and dc-photoconductivity (σ_{ph}) were measured as a function of temperature for the polycrystalline $(CdTe)_{100-x}(SbS)_x$ ($0 \le x \le 28$ at. %) thin films as shown in Fig. 9.

From this figure we can notice that, the conduction in these films is through an activated process having single activation energy in the temperature range from 300 to 400 K that can be expressed as $\sigma_{dc} = \sigma_0 exb(-\Delta E_{dc}/KT)$ where σ_0 is the pre-exponential factor, ΔE_{dc} is the activation energy for dc conduction, k is Boltzmann's constant and T is the absolute temperature. The values of σ_{dc}, σ_{photo}, σ_0 and ΔE_{dc} are inserted in Table 3. According to Mott and Davis [29], the conduction in $(CdTe)_{100-x}(SbS)_x$ thin films take place in the extended states and an increase in SeSb content increases the density of localized states.

As shown in Fig. 10, the variation of σ_{ph} of $(CdTe)_{100-x}(SbS)_x$ (where x = 0, 8, 16, 20 and 28 at. %) thin films with temperature, at applied electric field 4 x 10^5 Vm^{-1} and relative light intensity G = 1.0 (the ratio between the light intensity and the maximum light intensity) is used to obtain the activation energy for photoconduction (ΔE_{ph}).The values of ΔE_{ph} were calculated from the slopes of $\ln(\sigma_{ph})$ vs. 1000/T curves and listed in Table 2. From that table, we can see that, ΔE_{ph} is much smaller than ΔE_{dc} and both of them decrease with increase of the SeSb content.

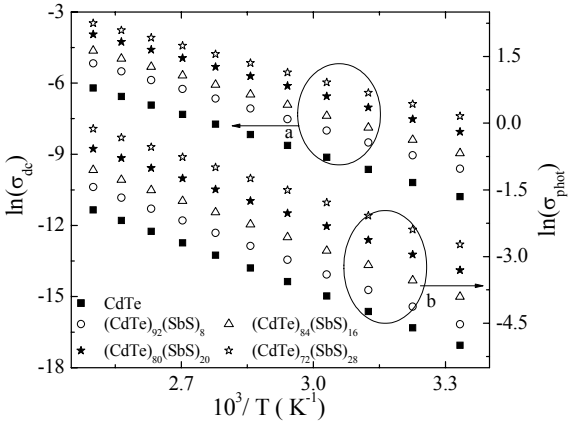

Fig.10. Temperature dependence of dc-dark and photoconductivity (at G =1.0 and applied electric field 4 x 10^5 Vm^{-1}) for $(CdTe)_{100-x}(SbS)_x$ ($0 \le x \le 28$ at. %) thin films

Table 3: The dc dark (σ_{dc}) and photo (σ_{ph}) conductivity, the pre-exponential factor (σ_0), the photosensitivity (σ_{ph}/σ_{dc}), the activation energy for dc dark (ΔE) and photo (ΔE_{ph}) conduction for $(CdTe)_{100-x}(SbS)_x$ ($0 \le x \le 28$ at. %) thin films.

SbS at. %	σ_{dc} ($10^{-5}\Omega^{-1}m^{-1}$) at 300K	σ_{photo}	$\sigma_{0\,(dc)}$ ($\Omega^{-1}m^{-1}$)	σ_{ph} / σ_{dc}	ΔE_{dc} (eV)	ΔE_{ph}
0	2.06	676	1890	328	0.485	0.315
8	6.67	1083	3591	162	0.459	0.313
16	12.98	2011	4161	154	0.446	0.294
20	31.92	3648	4322	114	0.423	0.282
28	75.29	6514	4878	86	0.404	0.268

The important parameter in the photoconductivity measurements is the photosensitivity (σ_{ph}/σ_{dc}) at a particular temperature and intensity. The value of (σ_{ph}/σ_{dc}) for a particular material decides the use of that material in photoconductivity devices. Therefore, the values of σ_{ph}/σ_{dc} of $(CdTe)_{100-x}(SbS)_x$ (where x = 0, 8, 16, 20 and 28 at. %) thin films at room temperature and G = 1.0 were calculated and inserted in Table 3. It is clear from this table that, the photosensitivity decreases with increase of the SeSb content. Although the dark current increases with increasing the SeSb content, the photocurrent does not increase by the same proportion. A decrease in the photosensitivity reflects an increase of the density of defect states in $(CdTe)_{100-x}(SbS)_x$ thin films with increasing the SeSb content. The photosensitivity depends upon the lifetime of excess carriers, which in turns depends upon the density of localized states in a particular material.

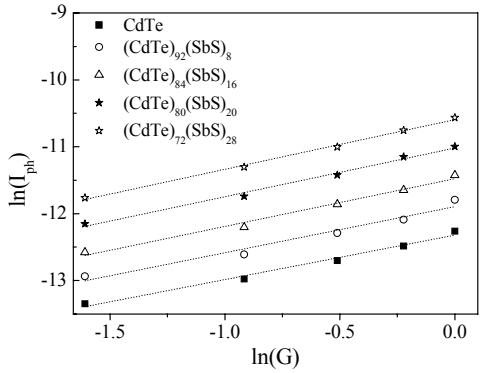

Fig.11. Dependence of photocurrent on relative light intensity at room temperature and applied electric field 4 x 10^5 Vm^{-1} for $(CdTe)_{100-x}(SbS)_x$ ($0 \le x \le 28$ at. %) thin films

The intensity dependence of photocurrent at room temperature and applied electric field 4 x 10^5 Vm^{-1} is shown in Fig. 11. The intensity dependence is found to obey the power law $I_{ph} \alpha G^{\gamma}$. The exponent γ determines whether the recombination process is monomolecular or bimolecular. In the single trap analysis [30], the exponent γ is equal to 0.5 for bimolecular recombination and 1.0 for monomolecular recombination. However, in case of continuous distribution of traps the value of γ lies between 0.5 and 1.0 [31]. The calculated values of the exponent γ lie between 0.5 and 1.0 (≈ 0.8) for all samples, that shows a continuous distribution of localized states in the mobility gap of these films.

4. Conclusions

In this paper, the compositional dependence of the dispersion parameters of polycrystalline $(CdTe)_{100-x}(SbS)_x$ (where x = 0, 8, 16, 20 and 28 at. %) thin films have been examined. Optical data indicated that the allowed direct gap is responsible for the photon absorption in the films. E_g^{opt} has been determined from the absorption coefficient in the form of $(\alpha h\nu)^2$ versus $h\nu$ (Tauc's formula) while, E_g^{photo} was obtained from the spectral dependence of the photocurrent. It was found that, the optical band gap and the single-oscillator energy decrease, while the refractive index and the dispersion energy increase with the progressive introduction of SbS in $(CdTe)_{100-x}(SbS)_x$ ($0 \le x \le 28$ at. %) thin films. The dispersion of the refractive index has been discussed in terms of the single-oscillator Wemple and DiDomenico and Solomon models. The study of dark and photoconductivity of the studied thin films as a function of temperature reveals that the conduction is through an activated process with single activation energy in the temperature range 300-400 K. The intensity dependence of photocurrent indicates the existence of a continuous distribution of localized states in the mobility gap of these films.

Acknowledgement

This work was funded by Physics department, Faculty of science, Al Azhar Univeresity, Assuit Branch, Assuit Egypt.

References

[1] A. Zakery, S.R. Elliott, J. Non-Crystalline Solid **330**, 1 (2003).

[2] A.B. Seddon, J. Non-Crystalline Solid **184**, 44 (1995).
[3] V. Sharma, A. Thakur, P. S. Chandel, N. Goyal, G. S. S. Saini, S. K. Tripathi, J. Optoelectron. Adv. Mater. **5**, 1243 (2003).
[4] K.A. Aly, A.M. Abousehly, A.A. Othman, J. Non-Cryst. Solids **354,** 909 (2008).
[5] M. A. Iovu, M. S. Iovu, E. P. Colomeico, J. Optoelectron. Adv. Mater. **5**, 1209 (2003).
[6] M. S. Kamboj, G. Kaur, R. Thangaraj, Thin Solid Films **420/421,** 350 (2002).
[7] Farid M. Abdel-Rahim, K.A. Aly, Tahani M. Shatir, J. All. Comp. **538**, 40 (2012).
[8] N. Kushwaha, R.K. Shukla, S. Kumar, A. Kumar, Mater. Lett. **60**, 3260 (2006).
[9] K.S. Bindra, N. Suri, P. Kumar, R. Thangaraj, Solid State Commu. **44**, 83 (2007).
[10] K.A. Aly, A.M. Abd Elnaeim, N. Afify, A.M. Abousehly, J. Non-Cryst. Solids **358,** 2759 (2012).
[11] R. Swanepoel, J. Phys. E: Sci. Instrum. **16**, 1214 (1983).
[12] R. Swanepoel, J. Phys. E: Sci. Instrum. **17,** 896 (1984).
[13] A. Dahshan and K.A. Aly, Acta Mater. **56,** 4869 (2008).
[14] S.A. Fayek, S.M. El-Sayed, NDT&E International **36**, 619 (2003).
[15] S. Velumani, Xavier Mathew, P.J. Sebastian, Solar Energy Materials & Solar Cells **76**, 359 (2003).
[16] V. Vassilev, M. Radonova, S. Boychev, Journal of Non-Crystalline Solids **356**, 2728 (2010).
[17] J.C. Manifacier, J. Gasiot, J.P. Fillard, J. Phys. E: Sci. Instrum. **9**, 1002 (1976).
[18] A. Dahshan, H.H. Amer and K.A. Aly, J. Phys. D: Appl. Phys. **41**, 215401 (2008).
[19] A. Dahshan, K.A. Aly, Phil. Mag. **89**(12), 1005 (2009).
[20] K. A. Aly, Appl Phys A **99**, 913 (2010).
[21] T.S. Moss, Optical Properties of Semiconductors, Buttenworths, London, 1959.
[22] K. Fajans, N. Kreidl, J. Am. Ceram. Soc. **31**, 105 (1948).
[23] S.H. Wemple, M. DiDomenico, Phys. Rev. **B3**, 1338 (1971).
[24] K.A. Aly, N.Afify, A.M.Aboushly, Physica B **405**, 1846 (2010).
[25] K. Tanaka, Thin Solid Films **66**, 271 (1980).
[26] I. Solomon, Phil. Mag. B **76**, 273 (1997).
[27] G.A.N. Connell, A.J. Lewis, Phys. Status Solidi b **60,** 291 (1973).e
[28] E.A. Davis and N.F. Mott, Phil. Mag. **22**, 903 (1970).
[29] N. F. Mott, E. A. Davis, Electronic Processes in Non-crystalline Materials, Ch 9, Clarendon Press, Oxford 1979.
[30] R. H. Bube, Photoconductivity of Solids, Wiley, New York, 1960.
[31] A. Rose, Concepts in Photoconductivity, Interscience, New York, 1963.

*Corresponding author: kamalaly2001@gmail.com,